Inorganic Chemistry
Article

Inorg. Chem. **2009**, *48*, 7165–7173 **7165**
DOI: 10.1021/ic9002115

ℝPM3: A Multifunctional Microporous MOF with Recyclable Framework and High H_2 Binding Energy†

Anjian Lan,[‡,§] Kunhao Li,[‡] Haohan Wu,[‡] Lingzhu Kong,[∥] Nour Nijem,[⊥] David H. Olson,[‡] Thomas J. Emge,[‡] Yves J. Chabal,[⊥] David C. Langreth,[∥] Maochun Hong,[§] and Jing Li*[,‡]

[‡]*Department of Chemistry and Chemical Biology, Rutgers, The State University of New Jersey, Piscataway, New Jersey 08854,* [§]*Fujian Institute of Research on the Structure of Matter, Chinese Academy of Sciences, Fuzhou, Fujian 350002, P.R. China,* [∥]*Department of Physics and Astronomy, Rutgers University, Piscataway, New Jersey 08854, and* [⊥]*Department of Materials Science and Engineering, University of Texas at Dallas, Richardson, Texas 75080*

Received February 2, 2009

A microporous metal organic framework structure, $Zn_2(bpdc)_2(bpee)\cdot 2DMF$ (DMF: *N*,*N*-dimethylformamide), has been synthesized via solvothermal reactions. The compound is a new member of the ℝPM series (ℝPM=Rutgers Recyclable Porous Material) that possesses a flexible and recyclable three-dimensional framework containing one-dimensional channels. It exhibits interesting and multifold functionality, including porosity, commensurate adsorption for hydrocarbons, high hydrogen binding energy (determined by isosteric heats of hydrogen adsorption and confirmed by van der Waals density functional calculations) as a result of multifold binding to aromatic ligands (determined by IR spectroscopy), strong photoluminescence emission, and reversible fluorescence quenching properties.

Introduction

We have recently reported a unique family of microporous metal organic framework structures that possess an interesting and useful structural property.[1,2] The ℝPMs (Rutgers Recyclable Porous Materials) have shown a complete reversibility of crystal-to-crystal structural transformation between a one-dimensional (1D) coordination polymer[3] and a porous three-dimensional (3D) network under very mild conditions. One very important application of these materials is their effective use as hosts in ship-in-bottle synthesis.[4] In such a process, reaction occurs inside the pore space (bottle) of the host and the product (ship) is difficult to be recovered (removed) from the host's internal surface. To "break the bottle", typically a concentrated acid or base has to be used to dissolve/rupture the host framework which would inevitably cause severe damage to the products.[5,6] We have demonstrated that when used as host in the photolysis of o-MeDBK (ship-in-bottle synthesis), the ℝPM-1-Co 3D framework breaks down readily and converts to 1D structure simply by immersing in water. This allows a full recovery of the products with a record breaking mass balance of 100%.[1]

In a continuing effort to develop new ℝPM materials with multifold functionality for other possible applications such as gas storage and separation, catalysis, and sensing,[7] we have successfully synthesized and characterized $[Zn_2(bpdc)_2(bpee)]\cdot 2$-DMF (DMF: *N*,*N*-dimethylformamide) (**1**) or ℝPM-3-Zn, a new member of the ℝPM family. Similar to ℝPM-1 and ℝPM-2, the framework of ℝPM-3 is highly flexible, and can be readily ruptured and rebuilt under very mild conditions. Employing three different methods, we have estimated the isosteric heats of hydrogen adsorption as a function of coverage. The high values obtained at low coverage suggest strong framework-hydrogen interactions in this compound, which is confirmed by van der Waals density functional calculations and IR absorption spectroscopic measurements.

† A. Lan and K. Li contributed equally to this project. This work is dedicated to Professor Xin-Tao Wu on the occasion of his 70th birthday.

*To whom correspondence should be addressed. E-mail: jingli@rutgers.edu. Phone: 732-445-3758. Fax: 732-445-5312.

(1) Pan, L.; Liu, H.-M.; Lei, X.-G.; Huang, X.-Y.; Olson, D. H.; Turro, N. J.; Li, J. *Angew. Chem., Int. Ed.* **2003**, *42*, 542.
(2) Pan, L.; Liu, H.-M.; Kelly, S. P.; Huang, X.-Y.; Olson, D. H.; Li, J. *J. Chem. Soc. Chem. Comm.* **2003**, 854.
(3) Pan, L.; Ching, N.; Huang, X. -Y.; Li, J. *Inorg. Chem.* **2000**, *39*, 5333.
(4) (a) Turro, N. *Acc. Chem. Res.* **2000**, *33*, 637. (b) Ramamurthy, V.; Garcia-Garibay, M. Zeolites as Supramolecular Hosts for Photochemical Transformations. In *Comprehensive Supramolecular Chemistry*; Bein, T., Ed.; Pergamon Press: Oxford, U.K., 1996; Vol. *7*.
(5) Corma, A.; Fornés, V.; García, H.; Miranda, M. A.; Sabater, M. J. *J. Am. Chem. Soc.* **1994**, *116*, 9767.
(6) DeWilde, W.; Peeters, G.; Lunsford, J. H. *J. Phys. Chem.* **1980**, *84*, 2306.
(7) (a) Maspoch, D.; Ruiz-Molina, D.; Veciana, J. *Chem. Soc. Rev.* **2007**, *36*, 770. (b) Custelcean, R.; Moyer, B. A. *Eur. J. Inorg. Chem.* **2007**, 1321. (c) Dinc, M.; Yu, A. F.; Long, J. R. *J. Am. Chem. Soc.* **2006**, *128*, 17153. (d) Cheetham, A. K.; Rao, C. N. R.; Feller, R. K. *Chem. Commun.* **2006**, 4780. (e) Rowsell, J. L. C.; Yaghi, O. M. *Angew. Chem., Int. Ed.* **2005**, *44*, 4670. (f) Kitagawa, S.; Kitaura, R.; Noro, S. *Angew. Chem., Int. Ed.* **2004**, *43*, 2334. (g) Janiak, C. *Dalton Trans.* **2003**, 2781. (h) Kepert, C. J. *Chem. Commun.* **2006**, 695. (i) Pan, L.; Parker, B.; Huang, X. Y.; Olson, D. H.; Lee, J.; Li, J. *J. Am. Chem. Soc.* **2006**, *128*, 4180–4181. (j) Pan, L.; Olson, D. H.; Ciemnolonski, L. R.; Heddy, R.; Li, J. *Angew. Chem., Int. Ed.* **2006**, *45*, 616. (k) Pan, L.; Sander, M. B.; Huang, X. Y.; Li, J.; Smith, M.; Bittner, E.; Bockrath, B.; Johnson, J. K. *J. Am. Chem. Soc.* **2004**, *126*, 1308.

Published on Web 07/02/2009

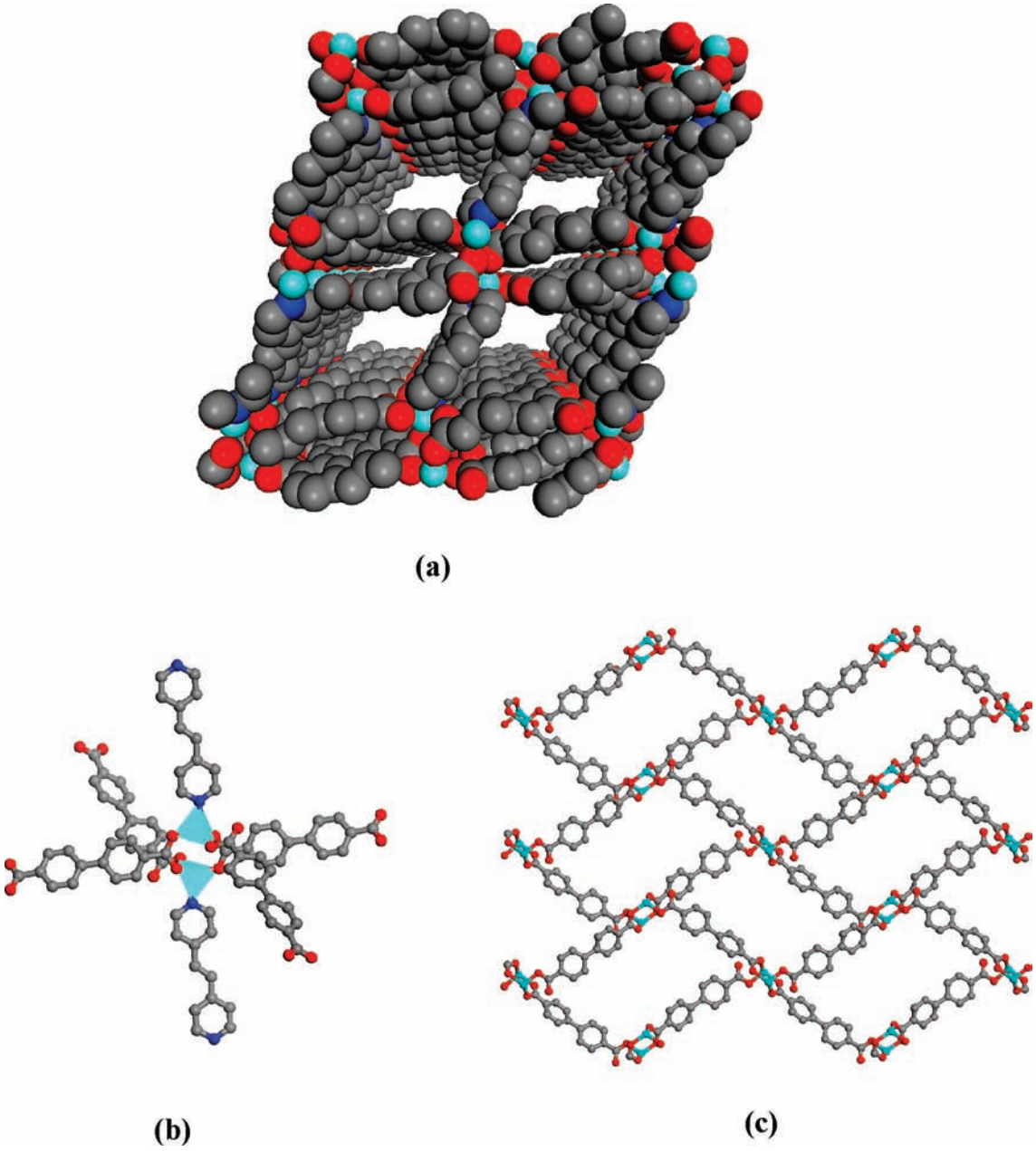

Figure 1. Crystal structure of **1′**. (a) The overall 3D framework. (b) The building unit in **1′**. The $Zn^{II}O_3N$ tetrahedra are indicated in aqua. (c) A single brick-like net (Zn: aqua; C: gray; O: red; N: blue).

Scheme 1. Removal and Reintroduction of Guest DMF, and the Reversible Structural Transformation between **1** (3D) and **2** (1D)

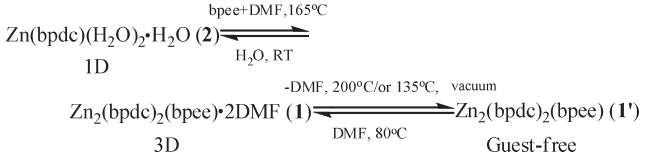

The compound also takes up a large amount of hydrocarbons and exhibits commensurate adsorption of benzene, *o*- and *p*-xylene, and potential for separation of the two xylenes. Strong photoluminescence is found in ℝPM-3-Zn and its solvent impregnated samples including anisole, toluene, benzene and chlorobenzene. Fast and reversible fluorescence quenching is observed when exposed to nitromethane, nitrobenzene, benzoquinone, dinitrotoluene (DNT), and dimethyl-dinitrobutane (DMNB, plastic explosive taggant) in the vapor phase. Such property may be useful in detection of trace vapor of explosives.

Results and Discussion

Crystal Structure. Single crystal X-ray diffraction performed on a selected crystal of **1** or ℝPM-3-Zn revealed that it is a microporous structure possessing a 3D network. As shown in Figure 1a, the network contains parallelogram-shaped 1D open channels running along the *b*-axis (window size: ~5×7 Å, excluding van der Waals radius of the carbon atom, 1.7 Å). All Zn atoms in the structure are tetrahedrally coordinated. The two carboxylate groups of each bpdc coordinate to Zn(II) centers in two different modes: one in μ_2 bidentate mode and the other in monodentate mode. Two such μ_2 bidentate carboxylate groups from two bpdc ligands that are opposite to each

other coordinate to two Zn(II) to form a eight-member ring $Zn_2(COO)_2^{2+}$ building unit (Figure 1b), and two monodentate carboxylates from another two bpdc bond to the two Zn (II) centers. Each $Zn_2(COO)_2^{2+}$ unit is further connected to four neighboring units to form a 2D brick-like net (Figure 1c). Two such (identical) nets interpenetrate to generate a layer. The adjacent layers are connected through bpee ligands to Zn (II) centers, completing the tetrahedral geometry for each Zn(II) (Figure 1b) and giving rise to the overall 3D structure. After removal of DMF solvent molecules filled in the pore space, the solvent accessible volume in **1′** or ℝPM-3′ was calculated to be 1171.9 Å^3 (27.6% of the unit cell volume).

Thermal Properties. Thermogravimetric analysis (TGA) of **1** showed 15.6% weight loss in the temperature range of 80−140 °C, in excellent agreement with the weight of guest DMF (calc 15.6%). The guest-free framework **1′** was found to be stable up to 400 °C (see Figure S1, Supporting Information). The guest DMF of a bulk sample (e.g., ∼100 mg) can be completely removed by heating the as-made sample at 135 °C under vacuum for 10−12 h, or by pumping under vacuum at room temperature following solvent exchange reactions with methanol (3 days) and dichloromethane (4 days) subsequentially. Structure integrity was examined following each treatment by powder X-ray diffraction. As shown in Figure S2 (Supporting Information), **1′** remains highly crystalline and retains main structural features but with shift of several peaks and appearance of a few new peaks. This is due to the distortion of the crystal lattice in response to the removal of guest molecules, commonly observed in many MOF structures. The PXRD analysis also confirmed that the structure of **1** was easily resumed by simply heating the guest-free sample of **1′** in DMF at 80 °C for 6 h. This conversion was much milder compared with the original reactions (165 °C, 3 days).

Reversible Structural Transformation. Structural transformation between **1** and a 1D structure [Zn(bpdc)-$(H_2O)_2]\cdot H_2O$[3] or **2** was observed, in a very similar way as in the cases of ℝPM-1 and ℝPM-2.[1,2] When immersed into distilled water for 2 h, **1** was converted completely into **2**, as indicated by PXRD patterns (see Figure S3, Supporting Information). The conversion from **2** back to **1** was achieved by heating the former with excess bpee in DMF solution at 165 °C for 3 days (Scheme 1).

Solvent Molecule Impregnations. Both **1** and **1′** were insoluble in common organic solvents. However, a number of solvent molecules, including anisole, toluene, benzene, and chlorobenzene can be impregnated into the 1D open channels within the framework, when samples of guest-free **1′** were immersed into these solvents under mild conditions (e.g., room temperature, 10 days). For nitrobenzene, slightly elevated temperature (at 80 °C, 30 h) was needed for impregnation to take place. All treatments were confirmed by TGA and PXRD. The weight-loss for anisole, toluene, benzene, chlorobenzene, and nitrobenzene impregnated samples (**3**, **4**, **5**, **6**, **7**) were 15.3%, 11.8%, 16.0%, 21.2%, and 12.7%, respectively, corresponding to ∼5.3, 4.6, 7.6, 7.6, and 3.8 anisole, toluene, benzene, chlorobenzene, and nitrobenzene molecules per unit cell, respectively (Figures S4−S8, Supporting Information). For benzene impregnation, the number of guest benzene molecules (7.6 per unit cell) is very close to the results of benzene adsorption measurement and simulation (8.0 per unit cell). For nitrobenzene impregnation, the number (3.8 per unit cell) is equal or very close to the results obtained from *p*- and *o*-xylene adsorption experiments (3.8 and 3.9 molecules per unit cell). The discernible inflection points (temperature at which the guest molecules are lost completely) are 160 °C, 120 °C, 110 °C, 135 °C, and 210 °C for anisole, toluene, benzene, chlorobenzene, and nitrobenzene impregnated samples, respectively, in good agreement with the boiling points (BP) of these molecules (156, 111, 80, 131, and 211 °C for anisole, toluene, benzene, chlorobenzene, and nitrobenzene, respectively).

Pore Characterization, Hydrogen Adsorption, and Binding Energy. The argon and nitrogen adsorption−desorption isotherms were measured at 87 and 77 K, respectively. A strong hysteresis accompanied with a "plateau" in the low pressure region of the adsorption branch was observed in both cases, but more severe for N_2 (see Figure S10, Supporting Information). Such observations can be explained well by pressure-dependent pore/gate-opening and pore/gate-closing phenomenon, reported in a number of other MOFs with similar structure features,[8] and are consistent with the fact that **1** is highly flexible, and can be readily regenerated from **1′** by heating in DMF at 80 °C for a few hours (Figure S2, Supporting Information). The surface area was estimated to be 328 m^2/g (BET) and 483 m^2/g (Langmuir), respectively. The total micropore volume was calculated to be 0.171 cc/g, indicating **1′** is a porous MOF with relatively small surface area and pore volume.

The hydrogen adsorption−desorption isotherms were measured at 77 and 87 K. As shown in Figure 2a, hysteresis was observed at both temperatures (pressure in the range of 0.001−1 atm), and is more severe at 77 K. This is usually attributed to insufficient equilibration time because of limited diffusion of adsorbate molecules in small pore materials, or quantum diffusion effect.[9] Longer equilibration time indeed led to reduced hysteresis at both temperatures, thus providing strong evidence for such effect. Consequently, the isosteric heats of hydrogen adsorption obtained from the adsorption branch will be underestimated, while those obtained from the desorption branch will be overestimated.[9] These data are plotted in Figure 2b as a function of H_2 coverage. For both adsorption and desorption branch, virial[10] and polynomial[11] methods were used for data fitting. Qst values

(8) Choi, H. J.; Dincă, M.; Long, J. *J. Am. Chem. Soc.* **2008**, *130*, 7848. Kitaura, R.; Fujimoto, K.; Noro, S. -I.; Kondo, M.; Kitagawa, S. *Angew. Chem., Int. Ed.* **2002**, *41*, 133. Kitaura, R.; Seki, K.; Akiyama, G.; Kitagawa, S. *Angew. Chem., Int. Ed.* **2003**, *42*, 428.

(9) Noguchi, D.; Tanaka, H.; Kondo, A.; Kajiro, H.; Noguchi, H.; Ohba, T.; Kanoh, H.; Kaneko, K. *J. Am. Chem. Soc.* **2008**, *130*, 6367. Zhao, X. B.; Xiao, B.; Fletcher, A. J.; Thomas, K. M.; Bradshaw, D.; Rosseinsky, M. J. *Science* **2004**, *306*, 1012.

(10) Czepirski, L.; Jagiello, J. *Chem. Eng. Sci.* **1989**, *44*, 797. Jagiello, J.; Bandosz, T. J.; Schwarz, J. A. *Langmuir* **1996**, *12*, 2837. Anson, A.; Jagiello, J.; Parra, J. B.; Sanjuan, M. L.; Benito, A. M.; Maser, W. K.; Martinez, M. T. *J. Phys. Chem. B* **2004**, *108*, 15820. Roswell, J.; Yaghi, O. M. *J. Am. Chem. Soc.* **2006**, *128*, 1304. Dinca, M.; Dailly, A.; Liu, Y.; Brown, C. M.; Neumann, D. A.; Long, J. R. *J. Am. Chem. Soc.* **2006**, *128*, 16876. Chen, B.; Zhao, X. B.; Putkhham, A.; Hong, K. L.; Lobkovsky, E. B.; Hurtado, E. J.; Fletcher, A. J.; Thomas, K. M. *J. Am. Chem. Soc.* **2008**, *130*, 6411.

(11) Lee, J. -Y.; Pan, L.; Kelly, S. K.; Jagiello, J.; Emge, T. J.; Li, J. *Adv. Mater.* **2005**, *17*, 2703. Lee, J. Y.; Olson, D. H.; Pan, L.; Emge, T. J.; Li, J. *Adv. Func. Mater.* **2007**, *17*, 1255.

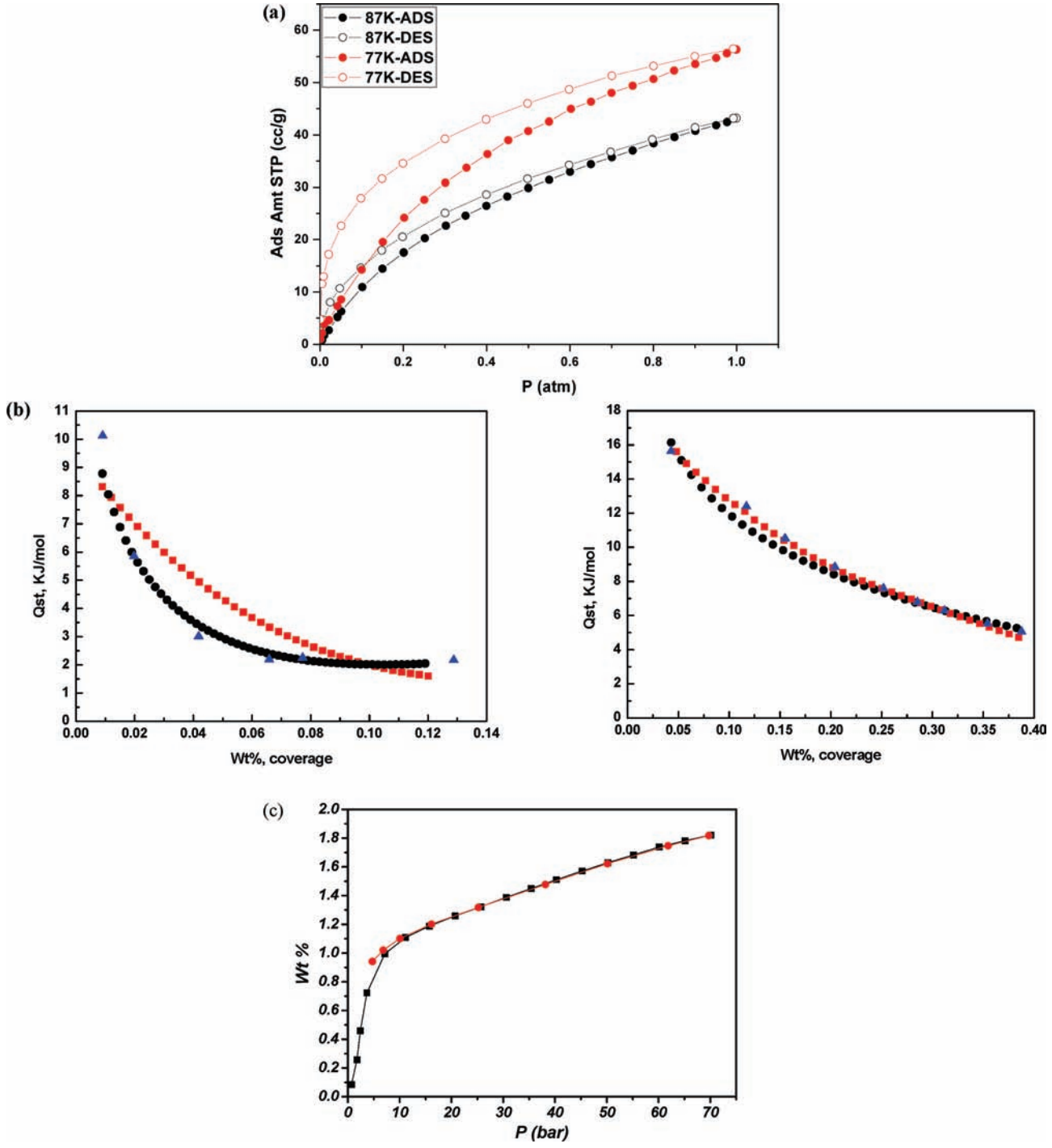

Figure 2. (a) Low pressure hydrogen adsorption−desorption isotherms at 77 and 87 K. (b) Isosteric heats of H_2 adsorption in **1′** from adsorption data (left) and desorption data (right). Color scheme: virial (red squares), polynomial (black circles), and experimental data by interpolation (blue triangles). No fitting was involved (AS1Win 2.01). (c) High pressure hydrogen adsorption (in black) and desorption (in red) isotherms at 77 K.

calculated directly from experimental data by interpolation using Quantachrome's software package (AS1Win 2.01) are also included. No fitting was involved in the latter case. For the desorption branch, all three data sets show remarkable agreement (Figure 2b, right) with Qst values reaching ∼14−16 kJ/mol at low loading and decreasing as the coverage increases. For the adsorption branch, however, significant deviations are found in the virial and polynomial sets between 0.02 and 0.08 wt %. The Qst values range between ∼8−10 kJ/mol at low loading. While accurate Qst values are not attainable in this case they certainly fall between the numbers given above from the two branches, and these values are comparable with the highest adsorption enthalpies reported to date, including 10.1 kJ/mol for $Co_4O(TATB)_{8/3}$ (TATB = 4,4′,4″-*s*-triazine-2,4,6-triyltribenzoate),[12] 9.4−10.4 kJ/mol for $NaNi_3(OH)(SIP)_2$ (SIP = 5-sulfoisophthalate),[13]

(12) Ma, S. Q.; Zhou, H. C. *J. Am. Chem. Soc.* **2006**, *128*, 11734–11735.
(13) Forster, P. M.; Eckert, J.; Heiken, B. D.; Parise, J. B.; Yoon, J. W.; Jhung, S. H.; Chang, J. -S.; Cheetham, A. K. *J. Am. Chem. Soc.* **2006**, *128*, 16846.

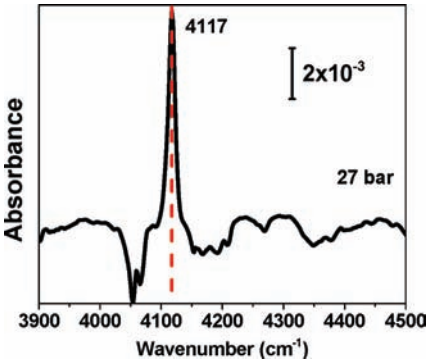

Figure 3. IR spectrum of H_2@**1′** measured at room temperature and referenced to activated **1′** in vacuum. The features appearing at the left and right of the main H_2 peak at 4117 cm^{-1} arise from the perturbation of the MOF structure upon H_2 loading.

10.1 kJ/mol for $[Mn(DMF)_6]_3[(Mn_4Cl)_3(BTT)_8(H_2O)_{12}]_2 \cdot 42DMF \cdot 11H_2O \cdot 20CH_3OH$,[14] 8.5−10.5 kJ/mol for metal exchanged $Mn_3[(Mn_4Cl)_3(BTT)_8(CH_3OH)_{10}]_2$ group compounds (zero loading),[15] 12.29 kJ/mol for $Zn_3(BDC)_3[Cu(pyen)] \cdot (DMF)_5(H_2O)_5$ at zero loading,[16] and 8.5−12.9 kJ/mol for M_2(dhtp) system (M = Zn, Ni).[17] It is also interesting to note a relatively high hydrogen uptake under higher pressures. A rapid increase was observed between 0 and 10 bar, followed by a nearly linear increase with significantly smaller slope. An uptake of 1.82% was achieved at 70 bar (Figure 2c). As a comparison, Zn(bdc)(ted)$_{0.5}$ has a Brunauer−Emmett−Teller (BET) surface area of 1794 m^2/g, about 5.5 times higher than that of **1′**.[11] Its maximum H_2 uptake is 4.1 wt %, roughly 2.2 times that of **1′**. The uptakes for O_2, N_2, and CH_4 at room temperature were found to be 7.01, 4.97, and 5.98 wt % at 70 bar, respectively.

To characterize the interaction of hydrogen with the ligands in **1′**, infrared spectroscopy measurements were performed at room temperature and high pressure (10−60 bar), using a KBr pellet to support ∼10 mg of **1′**. The H−H stretch frequency observed for H_2 incorporated in **1′** was measured at 4117 cm^{-1}, that is, with a 38 cm^{-1} red shift from the unperturbed ortho-ν(H−H) mode at 4155 cm^{-1} as shown in Figure 3. This shift is consistent with the interaction of H_2 with aromatic ligands. Interestingly, the intensity of the absorption mode is ∼5−6 times stronger than that measured in other MOFs (e.g., Zn(bdc)(ted)$_{0.5}$),[18] indicating that the interaction may involve multiple aromatic centers.

To understand the physical origin of the high isosteric heats of hydrogen adsorption and the vibrational spectra, we also performed first-principles calculations based on van der Waals density functional theory.[19,20] This approach has been very useful in locating the binding sites and understanding the MOF−H_2 interaction.[18] We used the new algorithm[21] (adapted from the Siesta code[22,23] for use in the Abinit code[24]), whose efficiency made a computation of this size easily manageable. A more detailed application of this method to the properties of a MOF will soon be available.[25] Here we first optimized the structure using the experimental structure of **1** (excluding the guest molecules) as our input. The optimized structure was then used for calculating the H_2 binding energies. Eight binding channels were discovered per unit cell with interaction energy of ∼15 kJ/mol, as sketched in Figure 4. These channels are located approximately midway between the two bpdc linkers and are aligned with the bpee linker. Each end of the channel is within a distance of ∼3.4−4.0 Å from three different linkers. The interactions between all three linkers (sites) and the hydrogen give rise to a strong binding energy of ∼12 kJ/mol, after subtraction of the zero-point energy from the interaction energy of ∼15 kJ/mol. This is consistent with the low loading Q_{st} values obtained from experimental hydrogen isotherms. We also calculated the H_2 stretch frequencies associated with these sites, finding shifts at the most strongly bound sites averaging ∼45 cm^{-1}, which are a bit larger than, but consistent with, the shifts found experimentally at room temperature (Figure 3).

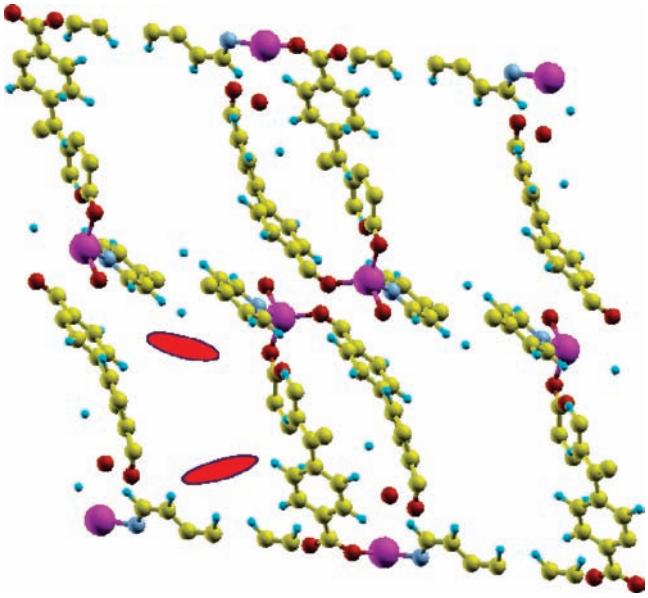

Figure 4. Highest energy H_2 binding regions within the conventional unit cell. These are marked in red, and also occur in the analogous regions in the three other sections of the cell.

(14) Dincă, M.; Dailly, A.; Liu, Y.; Brown, C. M.; Neumann, D. A.; Long, J. R. *J. Am. Chem. Soc.* **2006**, *128*, 16876.
(15) Dincă, M.; Long, J. R. *J. Am. Chem. Soc.* **2007**, *129*, 11172.
(16) Chen, B. L.; Zhao, X. B.; Putkham, A.; Hong, K. L.; Lobkovsky, E. B.; Hurtado, E. J.; Fletcher, A. J.; Thomas, K. M. *J. Am. Chem. Soc.* **2008**, *130*, 6411.
(17) Zhou, W.; Wu, H.; Yildirim, T. *J. Am. Chem. Soc.* **2008**, *130*, 15268.
(18) Kong, L. Z.; Cooper, V. R.; Nijem, N.; Li, K. H.; Li, J.; Chabal, Y. J.; Langreth, D. C. *Phys. Rev. B* **2009**, *79*, 081407(R).
(19) Dion, M.; Rydberg, H.; Schroder, E.; Langreth, D. C.; Lundqvist, B. I. *Phys. Rev. Lett.* **2004**, *92*, 246401.
(20) Dion, M.; Rydberg, H.; Schroder, E.; Langreth, D. C.; Lundqvist, B. I. *Phys. Rev. Lett.* **2005**, *95*, 109902.
(21) Roman-Perez, G.; Soler, J. M. arXiv0812.0244.
(22) Ordejón, P.; Artacho, E.; Soler, J. M. *Phys. Rev. B* **1996**, *53*, R10441.
(23) Soler, J. M.; Artacho, E.; Gale, J. D.; García, A.; Junquera, J.; Ordejón, P.; Sánchez-Portal, D. *J. Phys.: Condens. Matter* **2002**, *14*, 2745.
(24) (a) Gonze, X.; Beuken, J. -M.; Caracas, R.; Detraux, F.; Fuchs, M.; Rignanese, G. -M.; Sindic, L.; Verstraete, M.; Zerah, G.; Jollet, F.; Torrent, M.; Roy, A.; Mikami, M.; Ghosez, Ph.; Raty, J. Y.; Allan, D. C. *Comput. Mater. Sci.* **2002**, *25*, 478. (b) Gonze, X.; Rignanese, G.-M.; Verstraete, M.; Beuken, J.-M.; Pouillon, Y.; Caracas, R.; Jollet, F.; Torrent, M.; Zerah, G.; Mikami, M.; Ghosez, Ph.; Veithen, M.; Raty, J.-Y.; Olevano, V.; Bruneval, F.; Reining, L.; Godby, R.; Onida, G.; Hamann, D. V.; Allan, D. C. *Z. Kristallogr.* **2005**, *220*, 558.
(25) Kong, L.; Roman-Perez, G.; Soler, J. M.; Langreth, D. C. in preparation.

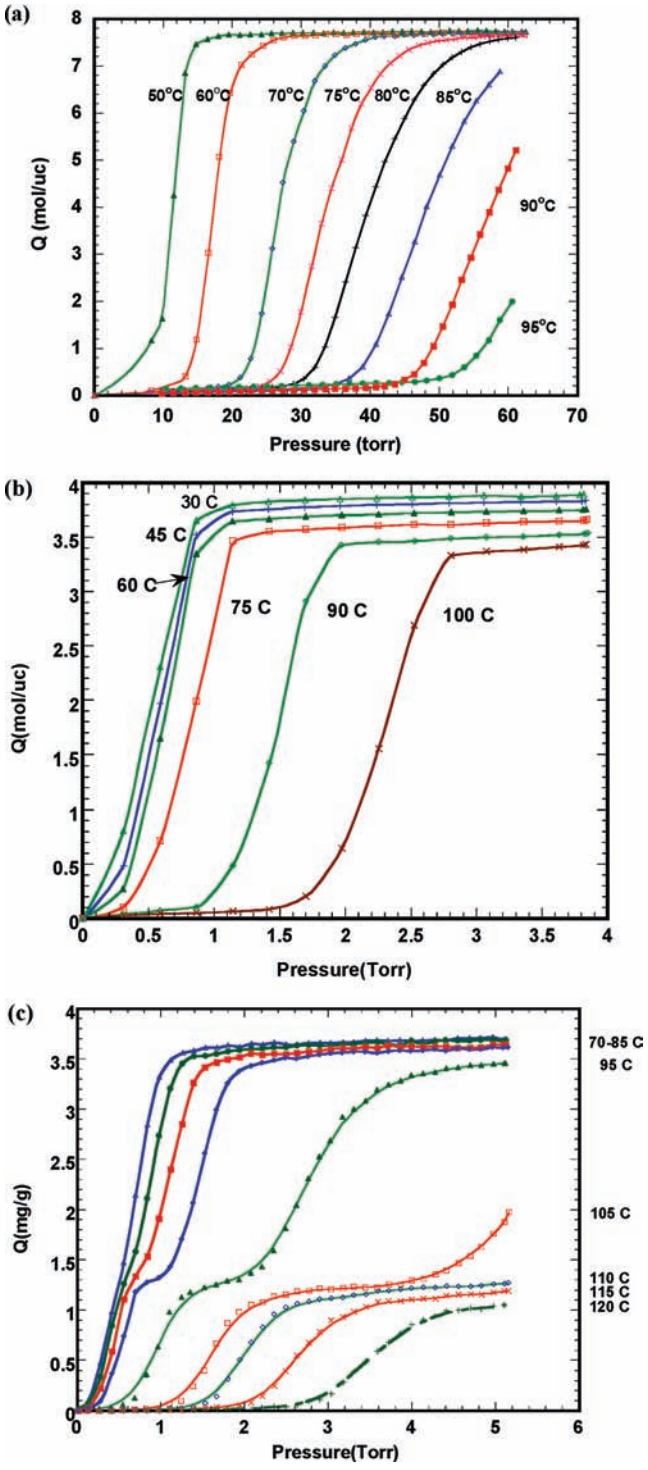

Figure 5. Adsorption isotherms of (a) benzene, (b) *o*-xylene and (c) *p*-xylene for a guest-free sample **1′** at several temperatures.

Each channel can accommodate two hydrogen molecules without much interference between them if we put one H_2 on each end of each channel. As such, the system adsorbs linearly up to 16 H_2 per unit cell, corresponding to about 1 wt %. Further loading leads to strong repulsion between the hydrogen molecules. This result agrees with the adsorption isotherm at 77 K plotted in Figure 2c which shows a rapid change when the loading is below 1 wt % and a slow increase after that, indicating the saturation of the eight primary sites at ~1 wt %. While there is agreement between experiment and theory for the maximum binding energy and the high pressure isotherm data, there is disagreement in the loading dependence of Q_{st}. Experimentally it was found that Q_{st} decreases more rapidly, while the theory predicts that the binding energy will remain at a high value until there are 16 hydrogen molecules per cell. This discrepancy is possibly related to the flexibility of the structure, mentioned earlier, but not taken into account in the theory.

Hydrocarbon Adsorption Properties. Adsorption curves at several temperatures for selected hydrocarbons (benzene, *o*-xylene, and *p*-xylene) are shown in Figure 5. These data reveal relatively high adsorption capacities of **1′**, for example, 192 mg/g for benzene which corresponds to a pore volume of 0.22 cc/g and is in reasonable agreement with the data obtained from argon sorption analysis. This pore volume is similar to the value 0.18 cc/g reported for the commercially important, medium pore size zeolite, ZSM-5.[26] The large pore zeolite, Y, has a pore volume of 0.29 cc/g.[27] All three hydrocarbons exhibit commensurate adsorption.[28,29] The room temperature experimental data suggest 8, 4, and 4 molecules per unit cell for benzene, *o*- and *p*-xylene, respectively. The benzene and *o*-xylene curves show classical type I behavior over the entire range of temperatures. *p*-Xylene has type I adsorption curves only for 70 °C and below. Above this temperature the curves convert to type IV and type V with a new, lower adsorption plateau at about 1/3 the value of the low temperature curves. This change may be due to a structural phase change although there is currently no supporting data for this phenomenon. Simple inspection of the *o*- and *p*-xylene adsorption curves suggest that conditions could be selected to achieve an adsorption preference of *o*-xylene over *p*-xylene. Competitive adsorption data are needed to determine the effectiveness of **1′** for gas separation.

Optical Emission and Fluorescence Quenching Effect. Optical emission properties of **1**, **1′**, and solvent-impregnated samples were investigated. The guest-free **1′** showed strong fluorescence emission (420 nm) in solid-state when it was excited at 320 nm (Figure 6). The photoluminescence experiments were also carried out on solvent-substituted samples under the same conditions. In most cases, strong emissions with a red-shift with respect to the emission wavelength of **1′** were observed, as shown in Figure 6. The magnitude of such red shifts is in the following order: **3** (62 nm) > **4** (23 nm) > **5** (9 nm) > **6** (6 nm), in accordance with the trend of the electron richness of the impregnation solvents.

The nitrobenzene-impregnated sample (**7**) was an exception. Nearly 100% fluorescence quench was observed upon excitation at 320 nm. Encouraged by this finding we conducted a systematic study to investigate the quenching effect of several selected chemical species, including explosives. Our investigation shows that **1′** exhibits very fast and highly sensitive fluorescence quench toward DMF,

(26) Roberts, R. E.; Rees, L. V. C. *Langmuir* **1987**, *3*, 335.
(27) Breck, D. W. *Zeolite Molecular Sieves*; John Wiley & Sons: New York, 1974.
(28) Olson, D. H.; Kokotailo, G. T.; Lawton, S. L.; Meier, W. M. *J. Phys. Chem.* **1981**, *85*, 2238.
(29) Li, K. H.; Olson, D. H.; Lee, J. -Y.; Bi, W. -H.; Wu, K.; Li, J.; Yuen, T.; Xu, Q. *Adv. Funct. Mater.* **2008**, *18*, 2205.

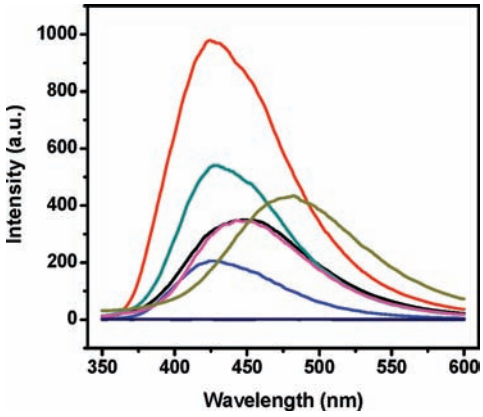

Figure 6. Fluorescence emission of as-made sample **1** (black), guest-free sample **1′** (red), and solvent-impregnated samples **3** (dark yellow), **4** (magenta), **5** (cyan), **6** (blue). Nearly 100% fluorescence quench was observed in nitrobenzene-impregnated sample **7** (navy, straight line).

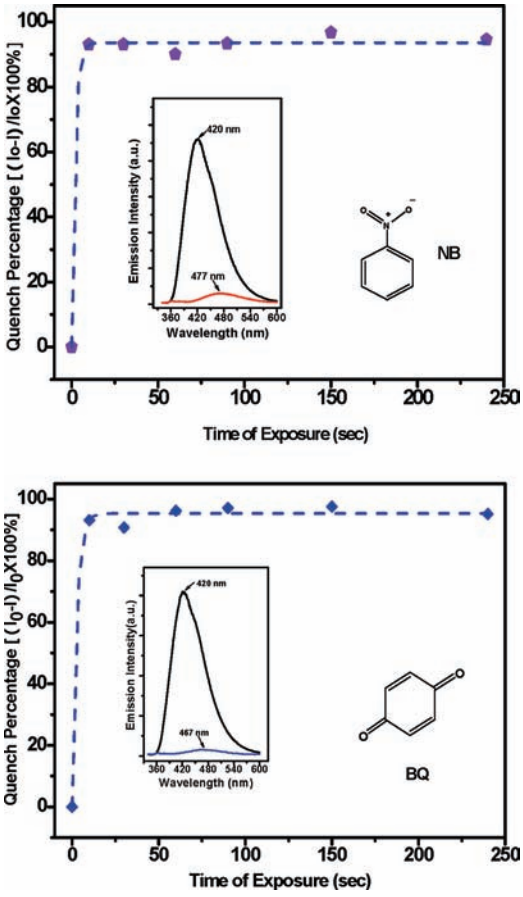

Figure 7. Fluorescence quenching percentage of nitrobenzene (top) and benzoquinone (bottom). The insets are fluorescence spectra before and after exposure to the analyte vapors for 10 s.

nitromethane, benzene, nitrobenzene, benzoquinone, DNT, and DMNB vapor. Depicted in Figure 7 are quenching effects of nitrobenzene (NB) and benzoquinone (BQ) at room temperature. In both cases, about 94–95% quench was achieved within 10 s of exposure to the vapor. For DNT and DMNB a 10 s exposure led to ~84% quench.[30] Most of the quench process was found

(30) Lan, A. J.; Li, K. H.; Wu, H. H.; Olson, D. H.; Emge, T. J.; Ki, W.; Hong, M. C.; Li, J. *Angew. Chem., Int. Ed.* **2009**, *48*, 2334.

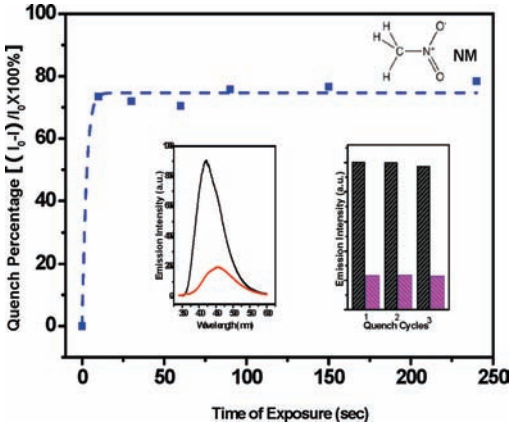

Figure 8. Fluorescence quenching percentage of nitromethane (NM). Inset plots are fluorescence spectra before and after exposure to nitromethane vapor for 10 s (left) and three continuous quench/regeneration cycles (right).

completely reversible. As an illustrative example, three consecutive cycles of quench/regeneration process for nitromethane (NM) are plotted in Figure 8. As shown in the inset plot, both the quench (exposed in nitromethane vapor for 10 s) and regeneration (heated at 100 °C for 1 min) process can be repeated to give almost identical results. These data suggest that the title compound and related materials may be potentially important candidates for use in fast and reversible detection of trace vapors of high explosives via fluorescence quenching techniques.

Conclusions

In conclusion, a new member of the ℝPM family has been synthesized and structurally characterized. $[Zn_2(bpdc)_2(bpee)]\cdot 2DMF$ (**1**) possesses a flexible and porous framework that can be ruptured and rebuilt under very mild conditions and via a fully reversible structure transformation to a 1D structure $[Zn(bpdc)(H_2O)_2]\cdot H_2O$ (**2**). The guest molecules of **1** can be removed and appropriate organic molecules can be impregnated reversibly into the pore space. The framework interacts strongly with hydrogen, primarily through three ligand sites at close proximity, resulting in a relatively high binding energy. This high binding energy is confirmed by both the IR measurements (~10 kJ/mol) and first-principles calculations based on van der Waals density functional theory (~12.5 kJ/mol).

The compound adsorbs a large amount of hydrocarbons and commensurate adsorption of benzene, *o*- and *p*-xylene is observed. The hydrocarbon adsorption study also indicates the possibility for use of **1** in gas separation. Strong emission is found in **1′**, and its solvent impregnated samples including anisole, toluene, benzene, and chlorobenzene. Fast and reversible fluorescence quenching by selected species, including DMF, nitromethane, nitrobenzene, benzoquinone, DNT, and DMNB (plastic explosive taggant) makes the title compound promising for applications in trace vapor detection of explosives and other relevant molecules.

Experimental Section

Materials. All chemicals were purchased from commercial suppliers (Alfa Aesar, Acros, Fluka, Fisher or TCI America) and used as received. The purity of benzene, *o*- and *p*-xylene used in adsorption experiments was 99.9%.

Synthesis, Solvent Exchange, Guest Removal and Reintroduction. Transparent block-like crystals of $Zn_2(bpdc)_2(bpee)\cdot 2$-DMF (**1**) were synthesized from a solvothermal reaction of $Zn(NO_3)_2\cdot 6H_2O$ (0.0892 g, 0.30 mmol), 4,4′-biphenyldicarboxylic acid (H_2bpdc, 0.0727 g, 0.30 mmol) and 1,2-bipyridylethene (bpee, 0.0547 g, 0.30 mmol) with molar ratio of 1:1:1 in a DMF (15 mL) solution. The reaction was heated at 165 °C in a Parr reaction vessel for 3 days under autogenous pressure and allowed to cool down to room temperature. Colorless crystals of **1** (0.0817 g, 58% yield) were isolated by filtering and washing thoroughly with DMF and ethyl ether. Solvent exchange reactions were carried out at room temperature by immersing a freshly made sample of **1** (0.050 g, 0.053 mmol) in methanol (10 mL, 3 days) and dichloromethane (10 mL, 4 days) consecutively, followed by pumping under vacuum to afford guest-free $Zn_2(bpdc)_2(bpee)$ (**1′**) (0.040 g, 95% yield). A mixture of **1′** (0.040 g, 0.050 mmol) and DMF (10 mL) was placed in a vial and heated at 80 °C for 6 h to afford **1** (0.045 g, 95% yield).

Reversible Structural Transformation. A freshly made sample of **1** (0.050 g, 0.053 mmol) was immersed into distilled water (10 mL) in a vial, followed by ultrasonic for 2 min. The sample was then placed in air for 2 h producing white powder of $Zn(bpdc)(H_2O)_2\cdot H_2O$ (**2**), the 1D chain structure[3] (0.035 g, 91% yield). The structure was converted back to **1** by heating **2** (the white powder, 0.018 g, 0.05 mmol) and bpee (0.018 g, 0.10 mmol) in DMF (15 mL) at 165 °C for 3 days which afforded block-like crystals of **1** with 64% yield (0.015 g).

Guest Molecule Impregnation. Four freshly made guest-free samples of **1′** (0.040 g, 0.050 mmol each) were immersed into 5 mL each of anisole (ANI), toluene (TOL), benzene (BZ), and chlorobenzene (CBZ) in 4 separate vials. The vials were placed at room temperature for 10 days, followed by filtering and washing with ethyl ether to produce $Zn_2(bpdc)_2(bpee)\cdot x$ANI (**3**), $Zn_2(bpdc)_2(bpee)\cdot x$TOL (**4**), $Zn_2(bpdc)_2(bpee)\cdot x$BZ (**5**), and $Zn_2(bpdc)_2(bpee)\cdot x$CBZ (**6**). A freshly made guest-free sample **1′** (0.040 g, 0.050 mmol) was immersed into nitrobenzene (NBZ, 5 mL) in a vial, heated at 80 °C for 30 h, followed by filtering and washing with ethyl ether to produce $Zn_2(bpdc)_2(bpee)\cdot x$NBZ (**7**).

Crystal Structure Analysis. Powder X-ray diffraction experiment was conducted using a D/M-2200T automated system (Ultima+, Rigaku) with Cu Kα radiation ($\lambda = 1.5406$ Å). The PXRD patterns were collected between 3° and 50° (2θ) at a scan rate of 4 deg/min (40 kV, 40 mA). Single crystal X-ray diffraction analysis was performed on a Bruker-AXS smart APEX I CCD diffractometer with graphite-monochromated Mo Kα radiation ($\lambda = 0.71073$ Å). A total number of 18781 reflections were collected (4349 unique, R(int) = 0.0474, $\theta = 2°-26.37°$), The structure was solved by direct methods and refined by full-matrix least-squares on F^2 using the Bruker SHELXTL package. $R1 = 0.0447$ ($I > 2\sigma(I)$), $wR2 = 0.1047$ (all data), GoF = 1.007 (all data). More details are provided in Table 1. Full listings of crystallographic data can be found in Supporting Information.

Thermogravemetric Analysis. The thermal properties of the compound were investigated using a TA Instruments Q50 TGA unit. An as-made sample of **1** (~8.7 mg) was loaded onto a sample pan and heated from room temperature to 600 °C at a rate of 20 °C/min under nitrogen (flow and purge rate at 40 mL/min and 60 mL/min, respectively).

Fluorescence Quenching Experiments. About 1.0 mL of nitromethane and nitrobenzene and 1.0 g of benzoquinone were each loaded in a small container. The small containers were then placed separately in three larger containers and set for 4 days (with the caps closed) to allow the vapor pressure of each analyte to reach equilibrium. Quartz slides (1.6 × 6 cm) were immersed into a mixture of deionized water and acetone and heated at 80 °C for 20 min, and then dried by nitrogen flow. Double-faced tapes (~ 1×2 cm) were stuck to the lower half of the quartz slides. The tapes were peeled off after a few minutes, leaving only residual glue on the quartz slides. The ground powder of **1′** was homogeneously sprinkled onto the area where double-faced tape had been stuck. Thin and relatively uniform layers (~5−6 μm in thickness) were obtained after tapping downward-facing quartz slides to remove any powder that was not glued well to the surface of the slides.

The room temperature fluorescence spectra of each sample on the quartz slides were collected before quenching occurred (the peak intensities of which were used to correct the effects of variations in layer thickness and morphology). To induce quenching, the slides were placed into the vapor atmosphere of each analyte for a designated time period (10 s, 30 s, 60 s, 90 s, 150 s, and 240 s). After the specified exposure time, each slide was taken out and quickly mounted to the sample holder, and the emission spectra were collected without delay. To examine the reversibility of the quenching effect for nitromethane, the fluorescence emission spectrum of sample **1′** was taken first and followed by three consecutive quenching (exposed in nitromethane vapor for 10 s) and regeneration (heated at 100 °C for 1 min) cycles.

Table 1. Summary of Crystal Data for **1**

empirical formula	C46 H40 N4 O10 Zn2
formula weight	939.56
temperature	293(2) K
crystal system	monoclinic
space group	$C2/c$
unit cell dimensions	
a, Å	26.1377(16)
b, Å	6.7464(4)
c, Å	25.0235(15)
α, deg	90
β, deg	105.916(1)
γ, deg	90
volume	4243.4(4) Å^3
Z	4
density (calculated)	1.471 Mg/m^3
absorption coefficient	1.195 mm^{-1}
final R indices [$I > 2$sigma(I)]	R1 = 0.0447, wR2 = 0.0969
goodness-of-fit on F^2	1.007

Gas and Hydrocarbon Adsorption. The high-resolution gas adsorption−desorption experiments were performed on a volumetric gas sorption analyzer (Autosorb-1 MP, Quantachrome Instruments). The cryogenic temperatures (77 and 87 K) were obtained using liquid nitrogen and liquid argon as coolant. Ultra high purity Ar (99.995%) and hydrogen (99.999%) were used for the experiments. The Ar sorption isotherms were collected in a relative pressure range from 10^{-6} to 1 atm at 87 K, and hydrogen sorption isotherms were collected in a relative pressure range from 10^{-3} to 1 atm at 77 K and 87 K. The initial outgassing process for each sample was carried out at 408 K for overnight (under vacuum). About 85−90 mg of degassed samples were used for gas sorption measurements, and the weight of each sample was recorded before and after outgassing to confirm the removal of guest molecules. The outgassing procedure was repeated on the same sample between experiments for 0.5−1 h. A total analysis time was about 3−4 days for Ar sorption and 15−20 h for hydrogen sorption. Pore properties (e.g., pore volume, pore size, and surface area) were analyzed using Autosorb v1.50 software. The high pressure volumetric gas analysis was performed by HPVA-100 (TA Instruments, FL) using H_2, N_2, O_2, and CH_4 of ultra high purity (99.999%). The same condition was applied to complete outgassing. Each isotherm was collected up to 70 bar using a sample of 708 mg.

Hydrocarbon adsorption measurements took place on a computer-controlled DuPont Model 990 TGA using the LabView program. The hydrocarbon partial pressure was varied by changing the blending ratios of hydrocarbon-saturated nitrogen and pure nitrogen gas streams.

Infrared Spectroscopy. The activated powder sample was pressed lightly onto a KBr pellet and inserted into a high pressure

cell. The high pressure cell was mounted into a Nicolet FTIR spectrometer, and measurements were done in transmission over the pressure range 400−900 psi at room temperature. The spectral range investigated is 500−5000 cm^{-1}, using a KBr beam splitter and Indium Antimonide liq. N_2 cooled detectors.

van der Waals Density Functional Calculations. Calculations were performed within the plane-wave implementation of the density functional theory in the ABINIT package which we have adapted to incorporate the van der Waals interaction.[18−24] We used Troullier-Martins pseudopotential with gradient corrected functional.[31] An energy cutoff of 50 Ry and Γ point sampling were found to be enough to converge the interaction energy within 0.1 kJ/mol and the frequency shift within 1 cm^{-1}.

The structure used in the calculations was determined by removal of the guest molecules, followed by relaxing that structure. The structure obtained is not identical to **1′**. It is very close to the as-make structure **1**, while the experimental guest-free structure (**1′**) shows changes. One such change is that the lowest order Bragg peaks occur at larger θ, suggesting a flatter cell with larger β. While the theoretical structure was essentially stress and force free, it possibly represents a different local minimum from that for the structure **1′**.

To calculate the vibrational frequency, we first preformed a series of total energy calculations with different H_2 bond lengths while keeping the center of H_2 and the MOF atoms at their equilibrium positions. The resulting total energies were used in the Schrödinger equation to obtain the eigenvalues, and the difference of the two lowest eigen levels gives the vibrational frequency.

Optical Excitation and Emission Experiments. The excitation and emission spectra of as-made, evacuated, and solvent exchanged samples were measured on a Varian Cary Eclipse fluorescence spectrophotometer. The excitation spectra were obtained by varying excitation energy while fixing the emission wavelengths at the emission maxima of the samples.

Acknowledgment. The financial support from DOE (Grant DE-FG02-08ER46491) is gratefully acknowledged. A.J.L. is thankful to the CAS/SAFEA International Partnership Program for Creative Research Teams for the financial support for his visit at Rutgers University. We thank Jose Soler for supplying us with an advance version of the code for his efficient algorithm for vdW-DF calculations. We also thank Dr. Matthias Thommes (Quantachrome Instruments) for many helpful discussions.

Supporting Information Available: Crystallographic data in CIF file format. TGA, PXRD patterns, optical absorption spectra, and gas sorption isotherms. This material is available free of charge via the Internet at http://pubs.acs.org.

(31) Troullier, N.; Martins, J. L. *Phys. Rev. B* **1991**, *43*, 1993.